ELECTRICAL ENGINEERING AND ENERGY

OPEN ACCESS

Optimal Sizing and Placement of Li-ion BESS for Virtual Inertia and Frequency Stability Enhancement in Grids with High Solar Penetration

Kaveke Kiima[1], Irene Muisyo[1], and Linus Aloo[1]

[1] Dept. of Electrical and Electronic Engineering, Jomo Kenyatta University of Agriculture and Technology, Nairobi, Kenya

Submitted: 11 April 2026
Accepted : 18 May 2026
Online First: 24 May 2026

Corresponding author
Kaveke Kiima,
kavekebrian3940@gmail.com

DOI:10.64470/elene.2026.30

Abstract: The global trend of large-scale high-capacity photovoltaic power generation has led to high instability due to inherent intermittency of solar energy and lack of mechanical inertia. Battery energy storage systems (BESS) as a solution can provide quick-response virtual inertia emulation (VIE). This study focused on the optimal combined sizing and location of lithium-ion BESS to achieve optimal virtual inertia supply and improve the frequency stability for grid networks with up to 40%-PV penetration. The optimization scheme aims to reduce the Life-Cycle Cost (LCC) and system penalties related to frequency deviations, the maximum frequency deviation and maximum allowable rate of change of frequency using the Teaching-Learning Based Optimization (TLBO). Simulations on modified IEEE 14 and 30 benchmark systems showed quantifiable benefits in optimal sizing of the assigned rating and capacities, namely the 44.4 MW and 193.9 MWh at Bus 8 on the 14-bus system, leading to significant attenuation of frequency deviation; in the 30-bus test case during a generator outage scenario, the frequency deviation was reduced from 0.503 Hz without BESS to 0.312Hz with BESS, and recovery time was reduced from 25s to 8s. In addition, the reliability indicators were improved, as shown with a decrease of the SAIDI index from 180 h/yr to 160 h/yr.

Keywords Frequency Stability, High PV Penetration, Li-ion BESS, Virtual Inertia Emulation (VIE).

1. Introduction

The world power generation is shifting to consider the environmental demands, advanced technology, and cost-effectiveness. The global capacity of renewable energy increased by 510 GW/year in 2023, approximated to 50% of that in 2022, and in 2024, this generation increased to 585 GW (International Renewable Energy Agency, 2025; Fernandez et al., 2006; International Energy Agency, 2023). However, when the penetration of solar PV is high, it presents unique stability challenges. Unlike synchronous generators, the PV arrays are connected to the grid via power electronic converters with no inherent rotational inertia (Piccoli et al., 2021). This often induces frequency transients, reducing reliability as the penetration increases. When the contribution of PV is greater than 40% the overall generation, grid inertia and frequency stability are significantly impaired (Islam et al., 2021).

Virtual Inertia Emulation (VIE) system, which integrate control mechanisms, inverters and energy storage systems (ESS) can be used to mimic the inertial response of synchronous machines (Islam et al., 2021; Julius et al., 2019). Among the ESS technologies, lithium-ion BESS is characterized by high energy and power density, quick response, high efficiency, and high scalability (Shahjalal et al., 2022). The complexity of an optimization problem, nonlinear dynamics, coupled spatial and time variables and very large search space, makes it necessary to use meta-heuristic algorithms (Golpira et al., 2020; Lybbert et al., 2021). The Teaching Learning Based Optimization (TLBO) algorithm has a faster convergence time, strong grid search behavior and low sensitivity to tuned control parameters compared to other algorithms (Rao & Patel, 2013; Zakeri & Askarian Abyaneh, 2017; Swetala et al., 2025). Large solar PV penetration can thus create significant frequency deviations and high RoCoF lowering reliability in grid systems. Although lithium-ion BESS can inject virtual inertia, the cost-effective and significant enhancement of frequency stability is dependent on the optimal selection of its size capacity and location placement on the grid (Basset et al., 2018). Improper sizing or location may lead to limited reliability, inflated costs and inability to achieve regulatory frequency variation and RoCoF thresholds (Swetala et al., 2025). Typically, the sizing or placement are considered separately (Shahjalal et al., 2022; Golpira et al., 2020). Furthermore, most optimization algorithms are limited by slow convergence, local optimum capture or parameter optimization. The optimization algorithm that effectively tunes the lithium-ion BESS sizing, and placement locations simultaneously is critical in achieving virtual inertia with minimal life-cycle cost and complying with grid stability requirements.

The stable frequency of the modern power grids is critical for its safe operation. The suitability of BESS to respond to a disturbance on the grid, however, is much dependent on the constraints of cost and maintaining Δf, RoCoF, and SoC limits (Basset et al., 2018). Conventional meta-heuristic methods like GA and PSO are computationally expensive, with slow convergence and highly sensitive parameterization thus the challenge when scaling to large systems. TLBO addresses these shortcomings, it requires only population size and a set number of iterations, providing faster convergence, and a desirable compromise between global and local search (Jaradat & Khatib, 2025; Abdel-Basset et al., 2018). Using TLBO and developing an objective function that considers both the cost and the stability indices, this paper develops a framework for integrating lithium-ion BESS into high-PV power systems for virtual inertia support. It jointly optimizes BESS size and placement, instead of treating them as separate problems. Lastly, it formulates an objective function that combines life-cycle cost with penalty terms for frequency deviation and RoCoF constraint violations. This paper is arranged into section as follows, the literature review, methodology, discussion of the results and conclusion.

2. Renewable Energy Integration

2.1 Impact of Renewable Energy Integration on Power System Inertia

The shift to high PV penetration sources, in grid system, introduces voltage variability and frequency regulation problems (Piccoli et al., 2021). System inertia, a critical feature of the power system, provides resistance to frequency fluctuations following a disruption by limiting RoCoF, thereby giving the operators time to take corrective action (Julius et al., 2019). While the conventional synchronous generators provide inertia in the rotating mass, solar PV are controlled by power-electronic converters that have no inherent inertial support, thus, increases frequency variability (Alam et al., 2022). Assuming constant power after a disturbance in a power system, the swing equation in (1), shows the relationship between power imbalance and the system frequency.

$$\frac{df}{dt} = -\frac{\Delta P}{2H} \tag{1}$$

Where ΔP is the magnitude of the power deficit, H is the equivalent inertia constant of the system (in

seconds), and df/dt is the rate of change of frequency. A decrease in the inertia constant H causes a linear increase in RoCoF, thus undermining stability. As Figure 1 indicates, a larger inertia constant (e.g., H= 6s), results in a smaller the frequency deviation and slower the RoCoF.

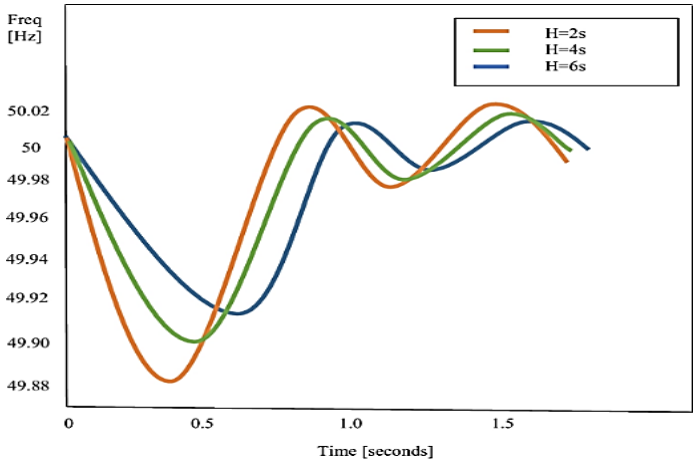

Figure 1: Impact of Inertia on frequency deviation (Ayamolowo et al., 2018).

Virtual inertia (VI) provides a solution to falling system inertia as the penetration of renewable sources exceeds 40% (Cai et al., 2022). The VI uses control mechanisms and energy storage systems (ESS) to emulate the dynamic behavior of asynchronous generators. The VI system measures grid frequency and calculates the necessary power injection or absorption through the ESS to overcome the deviations thus maintaining system stability (Neto et al., 2020). The primary benefits of VI are that it has faster response time, and increased efficiency. Conventionally, the VI control methods include virtual synchronous generators and synchronverters.

For higher effectiveness, the VI methods ought to have lower response time to correct frequency variations; a high-power density to permit rapid injection or absorption of large power; a long cycle life to withstand frequent charge -discharge cycles. It also needs a high round-trip efficiency (RTE) to minimize the energy loss and increase cost-effectiveness; low power cost and low energy cost to ensure financial feasibility; and a technology maturity to assure a proven performance, scalability, and reliability (Julius et al., 2019; Tamrakar et al., 2017). Lithium-ion batteries can be seen as a desirable solution to virtual inertia augmentation and represent an optimal compromise between fast response, power density, reasonable RTE, and the current technology and competitive pricing (Adetokun et al., 2022; Subasinghage et al., 2022).

2.2 Impact of BESS Size and Placement

A larger size of BESS can supply higher active power thus, a stronger, virtual inertial response, while mitigating the smaller frequencies and RoCoF effects. However, BESS placement of this magnitude increases the initial capital, operating and maintenance costs. Optimization is thus necessary to balance technical performance needs with economic feasibility (Julius et al., 2019). Furthermore, the placement of the BESS impacts its effectiveness. In cases where the BESS is located at nodes with high power-flow oscillations or with low interconnection strengths, the BESS has the maximum stabilizing effect on the frequency dynamics, and the lower RoCoF (Islam et al., 2021; Golpîra et al., 2020; Tercan et al., 2021). The optimal location would require a balance between the performance and the cost of the power system.

2.3 Optimization of BESS

Co-optimizing the size and placement of BESS is critical to maximizing high reliability while simultaneously minimizing the amount of storage capacity and capital costs. Conventional objective functions seek to minimize BESS capacity/cost, frequency deviation (Δf), RoCoF and frequency settling time. This objective

function are subject to operational constraints like limits on the Δf, RoCoF, BESS state-of-charge (SoC) and network power flow set limits. While conventional metaheuristic techniques like Particle Swarm Optimization (PSO), Genetic Algorithm (GA) and Simulated Annealing (SA) have been used to solve multi- objective problems (Tercan et al., 2021), they exhibit notable limitations. For instance, GA is associated with slow convergence and high computational cost; PSO suffers the entrapment at local optima, while SA is computationally expensive and often requires extensive parameter optimization.

An effective alternative is Teaching Learning Based Optimization (TLBO) algorithm which is inspired by the dynamics of classroom learning, with distinct teacher and student stages (Zakeri & Askarian Abyaneh, 2017; Abdel-Basset et al., 2018). Unlike the typical method, TLBO does not require algorithm-specific mutation rates or inertia weights, besides the low population size and the number of iterations. Also, the TLBO, as a two-step algorithm ensures a balance between the global exploration (teaching phase) and the local exploitation (student phase) (Zakeri & Askarian Abyaneh, 2017; Abdel-Basset et al., 2018). This averaging-based approach mitigates the premature convergence to local minimum and enhancing the solution quality on large search spaces.

3. Methodology

3.1 Modelling of the IEEE Bus Test Systems

Dynamic simulations were conducted using MATLAB software on IEEE 14 and 30 Bus test systems. Both systems were employed to simulate a base case without PV and BESS, PV-integrated case without BESS, and PV-integrated case with optimally placed BESS, including synchronous generation outages, and unanticipated line losses. The most important performance measures were frequency deviation and RoCoF across the buses (Alam et al., 2022).

3.1.1 IEEE 14 Bus Test System

To evaluate the proposed virtual control strategy, the IEEE 14 bus system was modeled into a test that included 5 synchronous generators, 11 load points, 3 transformers, and 20 transmission lines as in Figure 2 as a baseline (Abbawi et al., 2020). The integration points on PV were on buses 3, 6, 8 and 14 in IEEE 14-bus system. PV integration was largely formulated to account for 40% of the generation capacity commonly accepted as the base case of the optimization (Alam et al., 2022).

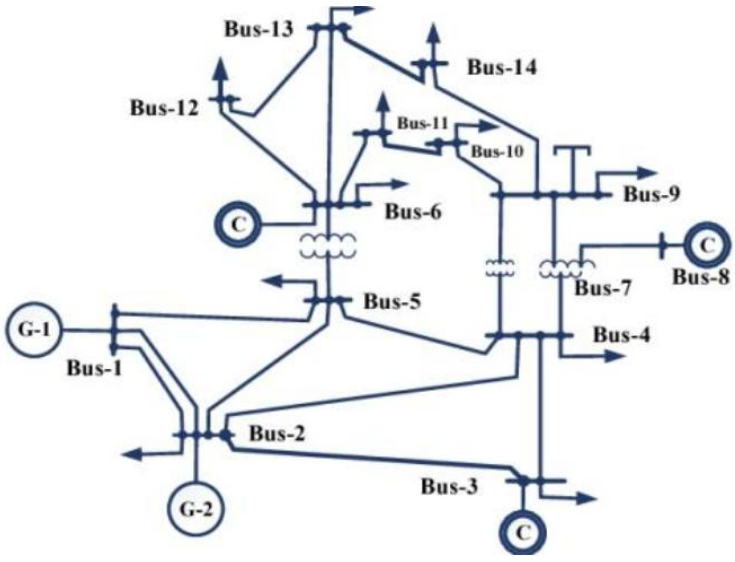

Figure 2 IEEE 14 bus Test system

PV penetration introduced to reduce effective system inertia and create stressed operating conditions for frequency-stability assessment. The candidate buses were evaluated under disturbance scenarios, and the BESS locations and ratings were determined by the TLBO-based optimization subject to frequency and RoCoF constraints.

3.1.2 IEEE 30 Bus Test System

The modelled IEEE 30 bus Test System had 30 buses, 6 generators, 3 synchronous condensers, 41 transmission lines and 20 load nodes. The integration points on PV were on buses 3, 7, 12, 15, 19, 21, 24, and 30 as in Figure 3 to account for 40% power generation. The modified IEEE 14-bus system served as the benchmark network for optimal BESS placement and sizing under the studied contingencies. The grid parameters include a frequency change limit range of 0.5 Hz, to 1.0 Hz. The corresponding RoCoF limits were 0.2/s -1 and 0.5/s -1 respectively [26]. The network capital costs were benchmarked at 1000 USD/kW and the 30 bus network capital cost estimates were 500 USD/MW and 200 USD/MWh utility-scale BESS (Cole et al., 2025).

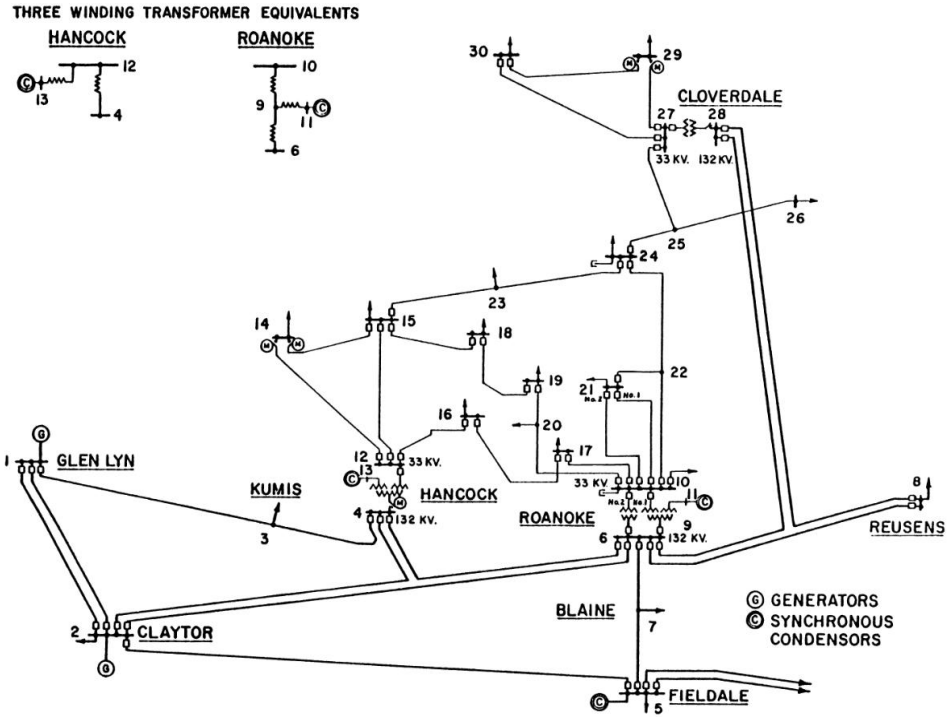

Figure 3 IEEE 30 bus Test system

3.2 Problem Formulation

3.2.1 Objective Function

The primary objective of optimal sizing is to reduce the Life-Cycle-Cost (LCC) of the BESS besides ensuring the placed units react quickly and efficiently to frequency variations. The multi-Objective Function, Minimize(X) was formulated as in (2)

$$Min\ F(X) = C_{LCC_{a,i}} + \lambda_1 (\Delta f_{max} - \Delta f_{limit})^2 + \lambda_2 (RoCOF_{max} - RoCOF_{limit})^2 \quad (2)$$

Where X is a decision variable consisting of the placement variable xi and the size variable $P_{BESS,i}$, $C_{LCC_{a,i}}$ is

the annualized Life Cycle Cost of each Li-ion BESS unit in $/kW-yr. The λ_1, λ_2 are penalty factors that determine the severity of violations of stability metrics. The Δf_{max} and Δf_{limit} are the maximum and regulatory limit for frequency deviation respectively, while $RoCoF_{max}$ and $RoCoF_{limit}$ are the associated frequency deviation constraints. The penalty coefficients λ_1 and λ_2 are utilized to strictly enforce physical grid limits, acting as high value weight (e.g. 1×10^6). If the simulated frequency deviation or RoCoF exceeds the regulatory thresholds (Δf_{limit} and $RoCoF_{limit}$), these weighted coefficients inflate the objective function, forcing the TLBO algorithm to discard sub-optimal or undersized BESS configurations that fail to support grid inertia.

3.2.2 Battery Energy Storage Systems (BESS)

When there is a BESS, the sum of total generation, which includes BESS generation, should be equal to the sum of all loads and transmission losses as in equation 3. Here $P_{gen,i}$ is the power from each of the N_g generation units, $P_{BESS,i}$ is the power from each of the N_b BESS units and $P_{load,i}$, P_{losses} at the load given N_l loads and total active power transmission losses across the network as in (3) [28].

$$\sum_{i=1}^{N_g} P_{gen,i} + \sum_{i=1}^{N_b} P_{BESS,i} = \sum_{i=1}^{N_l} P_{load,i} + P_{losses} \quad (3)$$

The operation of BESS state of charge is constrained by higher and lower limits to prevent accelerated degradation. To avoid both overcharging and deep discharging each instantaneous unit power, P_{BESS}, and energy, E_{BESS}, the set limit $P_{BESS,max}$, and $E_{BESS,max}$ ought to be maintained. The virtual inertia needed to counteract disturbances is used to determine the maximum allowable power of the BESS [28], which is given by, $P_{BESS,max}$. The dynamic SoC is based on the integrated power output over time, bounded by the minimum and maximum allowable limits.

During a disturbance, the magnitude of the frequency deviation depends on the imbalance between generation and load and the system's total inertia. The power imbalance is given by (4) [28].

$$P_{imbalance} = 2H_{eff}\, S_{base} x\, \frac{RoCOF}{f_0} \quad (4)$$

Where $P_{imbalance}$ is the instantaneous active power imbalance (MW), H_{eff} is the effective system inertia constant in seconds, S_{base} is the system base apparent power (MVA), f_0 is the nominal system frequency (Hz) and $RoCOF = \frac{df}{dt}$ is the rate of change of frequency (Hz/s). This swing equation shows that the instantaneous active power the BESS ought to inject or absorb to counter the kinetic energy deficit. The variation mimics the mechanical rotor thus effectively controlling the RoCoF before the frequency response of the grid is activated.

3.2.3 Stability Assessment and Placement Constraints

To maintain frequency stability, the BESS need to supply power to offset the power imbalance. The advantage of adding virtual inertia from Li-ion BESS is that it can counteract frequency deviations effectively by reacting much faster than synchronous generators that rely on inherent physical inertia through kinetic energy. The effective inertia constant of the system is given in (5).

$$H_{eff} = H_{sync} + H_{virtual\_BESS} \quad (5)$$

Where $H_{virtual\_BESS}$ and H_{sync} are the inertia provided by synchronous generators and BESS respectively. To evaluate the success of the virtual inertia, this study assessed the stability based on RoCoF, Nadir frequency and settling time. Besides, the optimization adhered to the spatial placement constraints defined in (6).

$$x_i \in \{0,1\}, \forall_i \in \{1,\ldots,N_b\};\ \sum_{i=1}^{N_b} x_i = k \quad (6)$$

Where x_i is A binary variable that indicates whether a BESS is installed at bus i, such $x_i = 1$ implies a BESS is installed at bus i and $x_i = 0$ means No BESS is installed at bus i, N_b is the total number of buses in the system with optimally placed k BESS units determined by the TLBO algorithm. The algorithm achieved k by balancing the number of weak buses, buses with converter interfaced renewable generation or critical loads.

3.2.4 Economic Analysis

The annualized life cycle cost $C_{\mathrm{LCC,a}}$ of Li-ion BESS is calculated as shown in (7).

$$C_{\mathrm{LCC,a}} = \sum_{m=1}^{N} C_{\mathrm{cap,a}} + \mathrm{C_{O\&M,a}} + \mathrm{R_{R,a}} \quad (7)$$

where $C_{\mathrm{LCC,a}}$ is the annualized LCC (\$/kW−yr), $C_{\mathrm{cap,a}}$ is the annualized total capital cost (TCC) per unit, $\mathrm{CO\&M_a}$ is the operation and maintenance cost per unit ($\mathrm{CO\&M_a}$) and $\mathrm{C_{R,a}}$ = replacement cost per unit, N is the Number of installed BESS units and $C_{\mathrm{cap,a}}$ is calculated as shown in (8).

$$C_{\mathrm{cap,a}} = TCC\ x\ CRF \quad (8)$$

where CRF is capital recovery factor and is given by (9).

$$\mathrm{CRF} = \frac{\mathrm{i(1+i)}^T}{\mathrm{(1+i)}^T - 1} \quad (9)$$

where i is the interest rate of borrowing money invested, T = lifetime of Li-ion BESS. The annualized operation and maintenance cost $\mathrm{C_{O\&M,a}}$ in \$/kW−yr is given by (10).

$$\mathrm{C_{O\&M,a}} = C_{FOM,a} + \mathrm{C_{VOM,a}} + \eta_{\mathrm{cycle}}\ \mathrm{x}\ T_{\mathrm{op}} \quad (10)$$

where $C_{FOM,a}$ is the annualized fixed operation and maintenance costs (\$/kW-yr), $\mathrm{C_{VOM,a}}$ is annualized variable operation and maintenance costs, η_{cycle} is the round-trip efficiency of BESS, and T_{op} is the charging and discharging cost of BESS. This equation models the running costs over the BESS lifespan, accounting for both the fixed yearly upkeep and the variable wear-and-tear induced by continuous charge-discharge cycling for frequency regulation.

The annualized replacement cost $C_{R,a}$ is given by (11).

$$C_{R,a} = CRF\ x\ \sum_{K=1}^{r}(1+i)^{-kt}\ x\ \frac{C_R x t_{ch}}{\eta_{sys}} \quad (11)$$

where CRF is the capital recovery factor, r is the Number of replacements during the lifetime, t is replacement period, η_{sys} is the overall system efficiency, t_{ch} is the charging duration and C_R is the replacement cost. The electrochemical degradation due rapid, high-power virtual inertia injections, demand that Li-ion cells must be replaced periodically. This equation calculates the present value of these future battery cell replacements, annualized to ensure the TLBO algorithm accurately minimizes long-term operational expenditures.

The inertia constant H in virtual inertia emulation is given by (12).

$$H = \frac{0.5\ x J_{VI}\ x\ \omega^2}{S_{base}} \quad (12)$$

where J_{VI} is the moment of inertia (kg.m²), ω is the angular velocity in rad/s, and S_{base} is the rated apparent power (MVA). This is a foundation equation for Virtual Inertia Emulation (VIE). It defines how the BESS control system transforms a measured grid frequency deviation into an equivalent kinetic energy response.

3.2.5 Energy Analysis

Given that stored energy in ESSs is usually expressed in volt ampere hour ($kVAh$), it can be converted into Joules (J) and then into kW using the relationships in (13) and (14) assuming a unity power factor. The relationship between the BESS power rating (P_{BESS} in MW), the discharge duration (h_{ESS} in hours), and the base power (S_{base}) is formulated as:

$$P_{BESS} = kW_{ESS} = kVA_{ESS} = \frac{h_{BESS}\, S_{base}}{3600} \tag{13}$$

$$h_{BESS} = \frac{3600\ x\ kVA_{ESS}}{S_{base}} \tag{14}$$

This equation gives the average hourly energy that can be injected or absorbed by the Li-ion BESS. The power of the P_{BESS} is, thus, given as in (15).

$$P_{BESS} = \sum_{i=1}^{n_{BESS}} \frac{h_i x S_{base}}{3600} \tag{15}$$

The equations (13), (14) and (15) define the physical energy bounds of the selected BESS. Since energy is power integrated over time, the optimization algorithm ought to ensure that the chosen battery unit possesses sufficient total energy capacity (MWh) to sustain the required maximum power injection (P_{BESS}) for the full duration of the transient disturbance, preventing premature depletion and ensuring strict adherence to State of Charge (SoC) constraints.

3.3 TLBO Implementation

Through the minimization of the objective function, the methodology favours Li-ion size and placement solutions that reduce required Li-ion BESS size, minimize life cycle costs and avoid frequency metrics violations. The objective function was solved using Teaching Learning Based Optimization (TLBO) algorithm. The algorithm operates by initializing, evaluating the fitness, and improving on it by the Teaching Phase (global exploration) and the Student Phase (local exploitation) as in the flow chart in Figure 4. For the implementation of the TLBO algorithm in MATLAB, the population size (N_p) was set to 50 learners. The maximum number of iterations (t_{max}) was set to 100 for the IEEE 14-bus test system and 150 for the IEEE 30-bus test system, as these limits allowed the algorithm to demonstrate rapid improvement and avoid premature convergence. Furthermore, the bounds for the decision variables during optimization were strictly set based on typical utility-scale parameters; the individual BESS power capacity bounds (P_{BESS}) were constrained between 15 MW and 50 MW per unit, and the energy capacity bounds (E_{BESS}) were constrained to maintain practical discharge durations between 0 MWh and 200 MWh per unit.

The output provides the optimum BESS sizes, which is $P_{BESS_{opt}}$, and optimal locations, which is x_{opt}. TLBO is used to optimise frequency stability of the selected buses in terms of cost minimisation and frequency metrics violation avoidance.

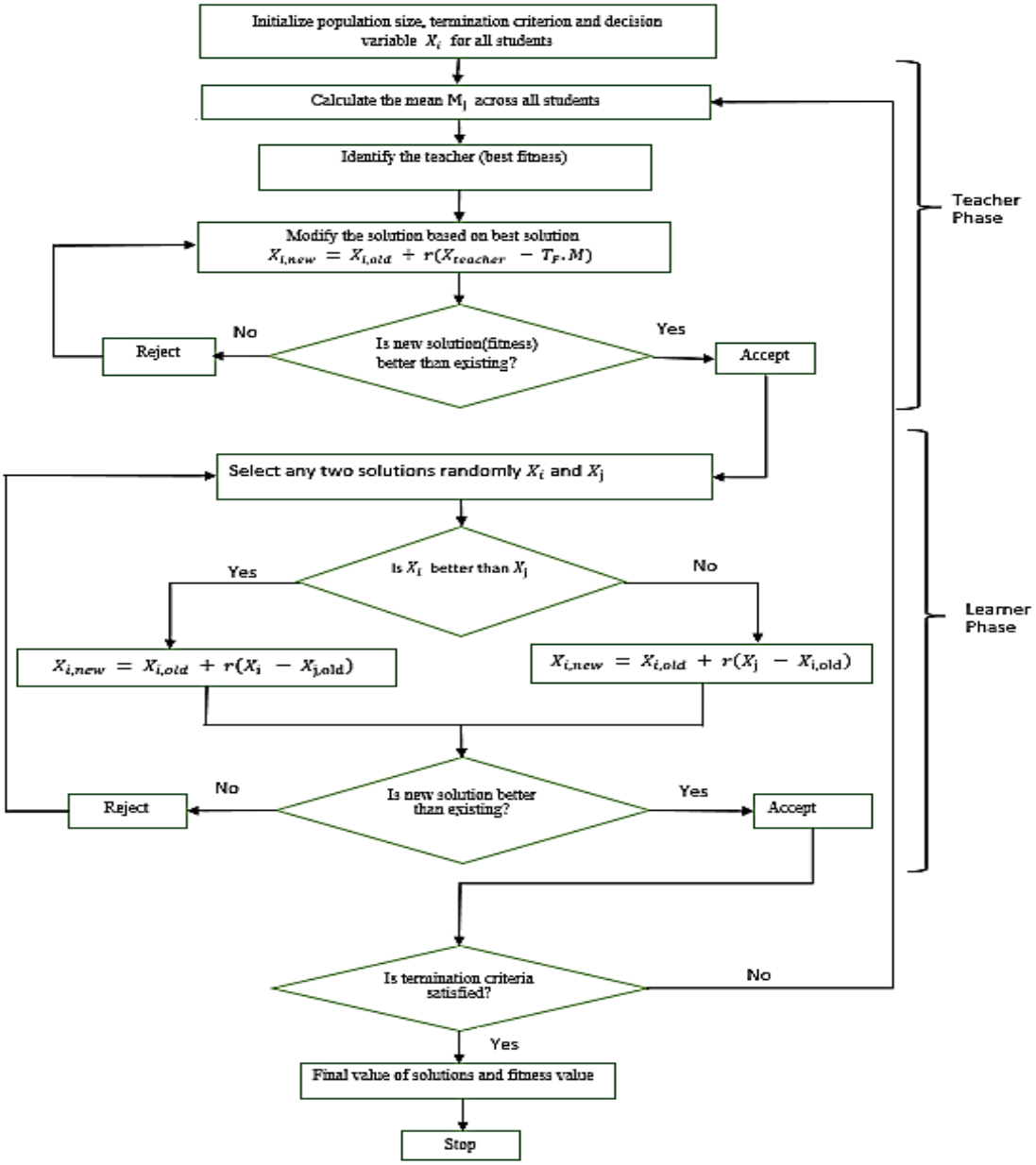

Figure 4 Flowchart of TLBO

3.4 Test Case for critical load

Critical loads were assigned to selected buses to evaluate the practical resilience value of the optimized BESS under contingency conditions. They included high-priority facility profiles, consistent with standard industrial power density benchmarks (Carpinelli et al., 2024; International Renewable Energy Agency, 2025) and assumptions as in Table 1. The critical load facilities were mapped on particular buses of the adjusted IEEE networks as a simulation of the real-world demand.

Table 1 Test case for critical load and assumptions

Facility Type	Load (MW)	Assumption
Hospital	12 MW	A typical inpatient facility requires approximately 2.5MW of reserved power; thus, a 12MW could run trauma unit.
Data Center	15 MW	The data center is categorized into industry classifications that are between 10MW and 70MW and a rating at 15MW was chosen.
Emergency	8 MW	This case is equivalent to single fire station that combines critical services such as fire dispatch, and municipal backup.
Industry	25 MW	Large industries like chemical processing regularly operate above 20MW per site.
Residential	18 MW	A practical load, an 18 MW corresponds with a critical feeder of a residential area with an estimated 1 MW per 600 households was assumed.

4. Results and Discussion

4.1 Overview

To test the proposed simultaneous sizing and placement two test systems, IEEE 14-bus and IEEE 30-bus networks were simulated. IEEE 14-bus system was used as a standard system to verify the effectiveness of the Teaching-Learning-Based Optimization (TLBO) algorithm on a standard network. The IEEE 30-bus system was used to confirm the scalability and strength of the algorithm on a bigger and transmission network characteristic of the modern operations. The simulations were performed with high penetration of solar PV between 20% and 50% to ensure that the inertial response of the grid was stressed. To evaluate the Virtual Inertia Emulation (VIE) of the optimized Li-ion BESS, we simulated four contingency situations, which are generator outage, line N-1 loss, PV power drop, and a step load. These conditions were chosen to test the system resilience in response to abrupt loss of rotating mass, topological transition, rapid variability of renewable sources and demand bursts.

4.2 IEEE 14-Bus

4.2.1 BESS Optimization

TLBO optimization of the IEEE 14-bus system was found to converge on a solution using 3 BESS units. Bus 8 was identified by the algorithm as the highest optimal placement for the inertial support at a power rating of 44.4 MW and an energy capacity of 193.9 MWh. A secondary and smaller unit were placed on Bus 1 (4.9MW/34.7MWh) and Bus 13, in third place (~0.0MW 36.5MWh) in respective units as shown in Figures 5(a) and 5(b) respectively. This optimization verifies that Bus 8 could be used as dominant support node paired with an auxiliary node on Bus 1 to arrest the RoCoF.

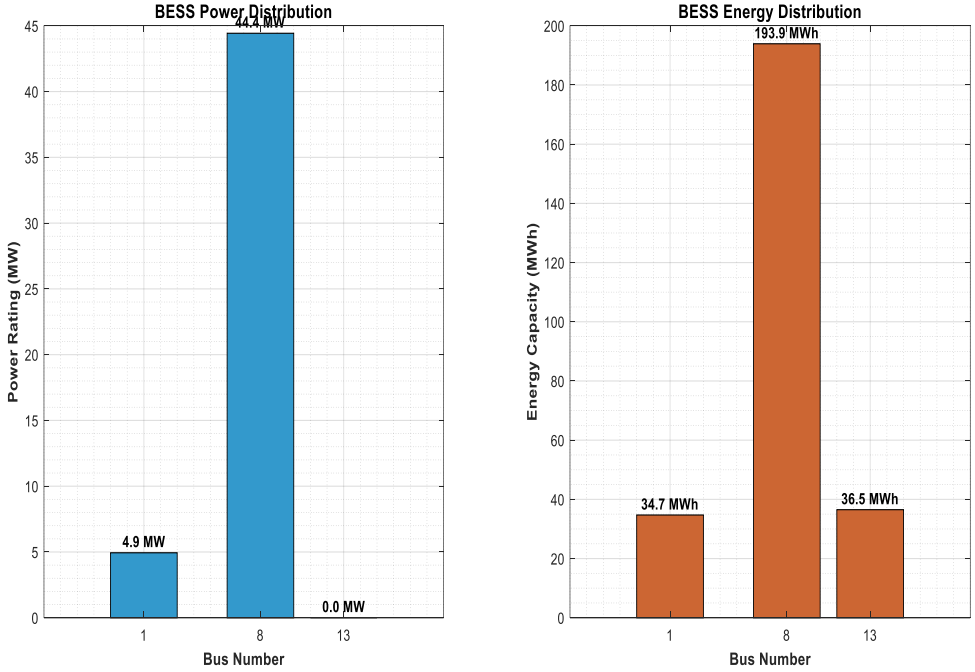

(a) (b)

Figure 5 IEEE 14-Bus (a) BESS Placement based on the power rating, (b) associate energy capacity on power distribution system

4.2.2 TLBO Analysis

Figure 6 illustrates the convergence of the TLBO algorithm in optimal placement and sizing of BESS for the IEEE 14-bus system. Figure 6(a) reveal both the TLBO Convergence Characteristics on a semi-logarithmic scale for objective function value versus iterations (0 to 100). The best fitness starts from about 2 and plateaus at about 0.1, after 60 iterations, showing rapid improvement while the worst fitness starts from a higher number 4.5 and decreases irregularly to 2. The steep trajectory highlights the TLBO algorithm's effectiveness in global exploration during it teaching phase. The population diversity percentage versus iterations plot in Figure 6(b) starts at 100% and descends to near 0, with concentration near the optimal solution. The localized oscillations depict the TLBO's learner phase ability to maintain local search permutations preventing premature entrapment in local minima before convergence. These results confirm that TBLO successfully places the BESS optimally given the special, dynamic and economic constraints.

4.2.3 Dynamic Response in Frequency and RoCoF

This Figure 7 demonstrates the transient response of the IEEE-14 Bus to a generator outage at t = 1 second. Post the generator outage, the frequency response curves in figure 7(a) show, the baseline 14-bus network without the BESS) with a highest frequency variation at 70Hz. For the case with base placement BESS the marginal deviation in frequency was about 15hz. For the RoCoF curve in Figure 7(b) the system with no BESS placement recorded a peak of 11 Hz/s at 6.5 seconds, while the corresponding peak was ~3 Hz/s. This implies that optimize BESS placement injected virtual inertia is almost identical to that of the baseline, but with limited transients. Comparing the Nadir frequency changes, it was highest when the generator outage at 10 HZ with no BESS, against 1HZ with corresponding case with optimized BESS placement for PV. Furthermore, the BESS placement lower Nadir frequency to ~0.043 Hz in a N-1-line loss and ~0.03 Hz in PV power drop contingencies as shown in Figure 7(c). The BESS placement is thus critical during the recovery phase. On the frequency recovery time, with the baseline scenario, the system stabilizes after 25 seconds compared to 8 seconds when optimal BESS placement is applied for generator outage. The quicker

recovery time points to faster restoration of the system to steady-state. These dynamic responses reveal the optimal BESS placement make the baseline system robust and quickly stabilizes the system.

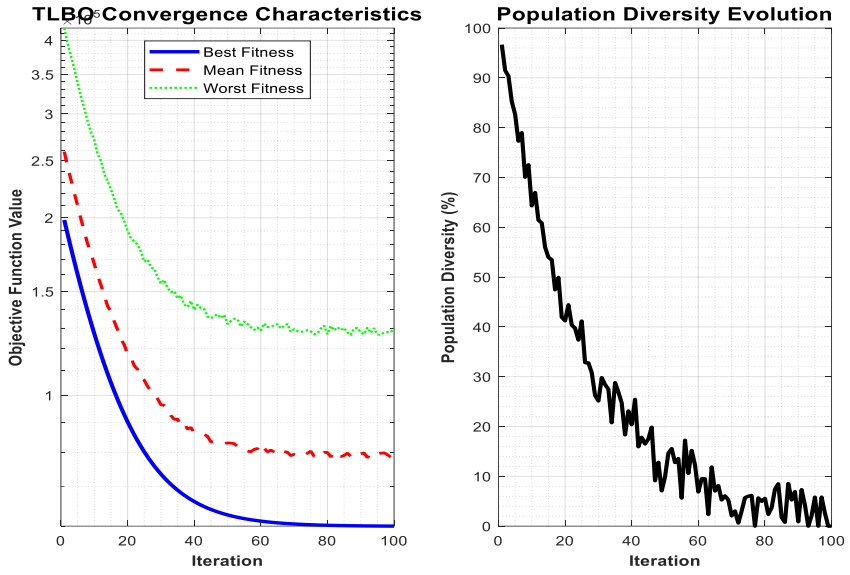

(a) (b)

Figure 6 (a) TLBO Convergence Characteristics, (b) Population Diversity Evolution for the IEEE 14-bus system

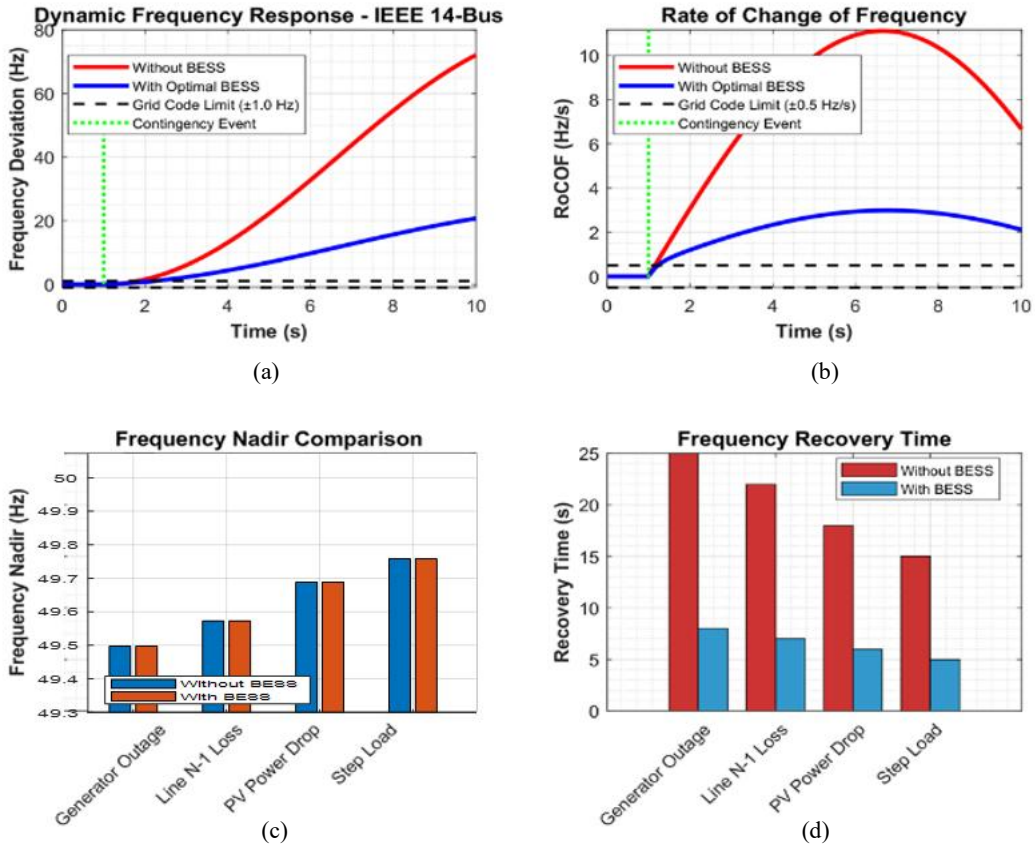

(a) (b) (c) (d)

Figure 7 (a) The dynamic frequency response in the IEEE 14-bus system, (b)) the rate of change of frequency, (b) The comparison of Nadir frequency at different contingency scenarios and (d) Frequency recovery at different contingency scenarios.

4.2.4 Reliability and Resilience analysis

Figure 8 shows the relative improvement in system reliability and resilience due to the optimal BESS placement of PV to the IEEE 14-bus system. In particular, the System Average Interruption Duration Index (SAIDI) declines on average of between 60 and 70 minutes a year down to a 180-minute base.

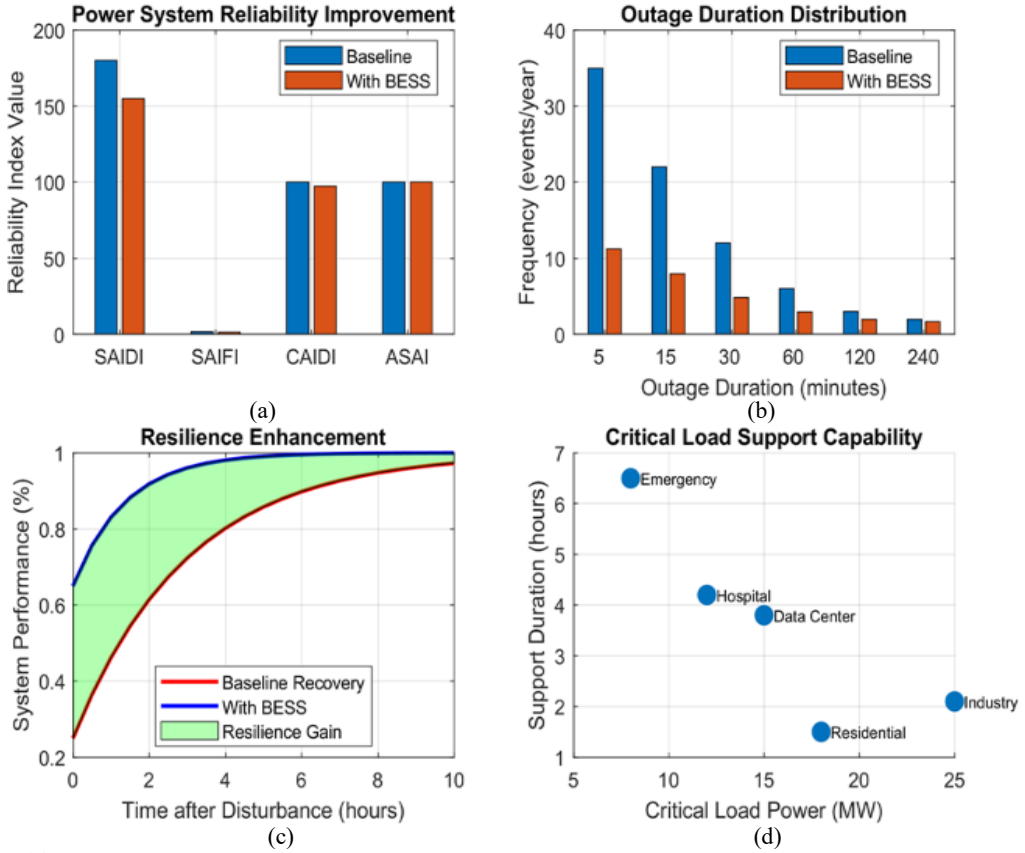

Figure 8 (a) The impact of BESS on system reliability for IEEE 14 Bus, (b) the outage distribution frequency against the duration of the outage, (c) resilience gain on the IEEE 30-bus system and (d) the critical load support capability.

There is an approximate reduction in the System Average Interruption Frequency Index (SAIFI) of 50-60 per cent, to a lower level of 0.7- 0.9 interruptions/annum. As a result, the storage integration is very close to an ideal reliability with an Average Service Availability Index (ASAI) of 99.98. The frequency of the duration of outage is also positively affected by the storage integration. The five-minute durations of outage decreased from 35 to about 26 cases per year. Moreover, blackouts of 240 minutes or more were eliminated, as reflected in the average of between 4 to 1.9 incidents per year. Resilience and critical load support analysis as a resilience criterion illustrates the ability of the system to carry isolated critical loads in a long period of contingency conditions. According to the BESS energy capacity, which is optimized, one can supply an 8 MW emergency service load, a 12 MW hospital, a 15 MW data center, a 25 MW industrial facility, and an 18 MW residential feeder with independent backup power of 6.5 hours, 4.2 hours, 3.8 hours, and 1.5 hours, respectively.

4.2.5 Grid Integration and Frequency Stability Analysis

Figure 9 shows the grid integration and power quality improvements in the steady-state enhancement through the best-suited Battery Energy Storage System (BESS) in the IEEE 14-bus network. Although the baseline mechanical inertia constant is believed to be adequate at 4.0 seconds, virtual inertia, which is mathematically calculated as the product of an equivalent 4.0 seconds of control gain applied to the 49.4

MW aggregate inverter capacity. Meanwhile the inverter-based control acts proactively to control the local electrical properties; at structurally weak nodes where the baseline voltages drop below 0.95 per-unit (p.u.). The optimal BESS placement raises local voltage profiles by around 0.04 p.u. to keep the network within the 0.95 to 1.05 p.u. allowable range. Moreover, the spatial distribution of this capacity allows for balanced power flow distribution throughout the grid so as to alleviate transmission losses during active power injection. The heavy capacity at Bus 8 is integrated seamlessly with the minor capacity at Bus 1 as shown in Figure 9(b). The power optimal placement of BESS enhances the active harmonic filtering, which reduces the voltage Total Harmonic Distortion (THD) of odd harmonic distortions by an estimated 16%. This is evident when the 5th and 3rd harmonics dropped from 3.2% and 2.7% to 2.1% and 1.8%, respectively. The 14-bus baseline system provides a mechanical inertia constant of the baseline system of H = 4.0s. This system's inertia is increased by the optimized BESS placement to ~23 s. When converted to the corresponding synthetic inertia contribution by virtual synchronous control loop of (12), corresponds to 4.0 seconds (calculated using the designed control gain of $0.08s/MW x 49.4MW ~= 3.95 s).

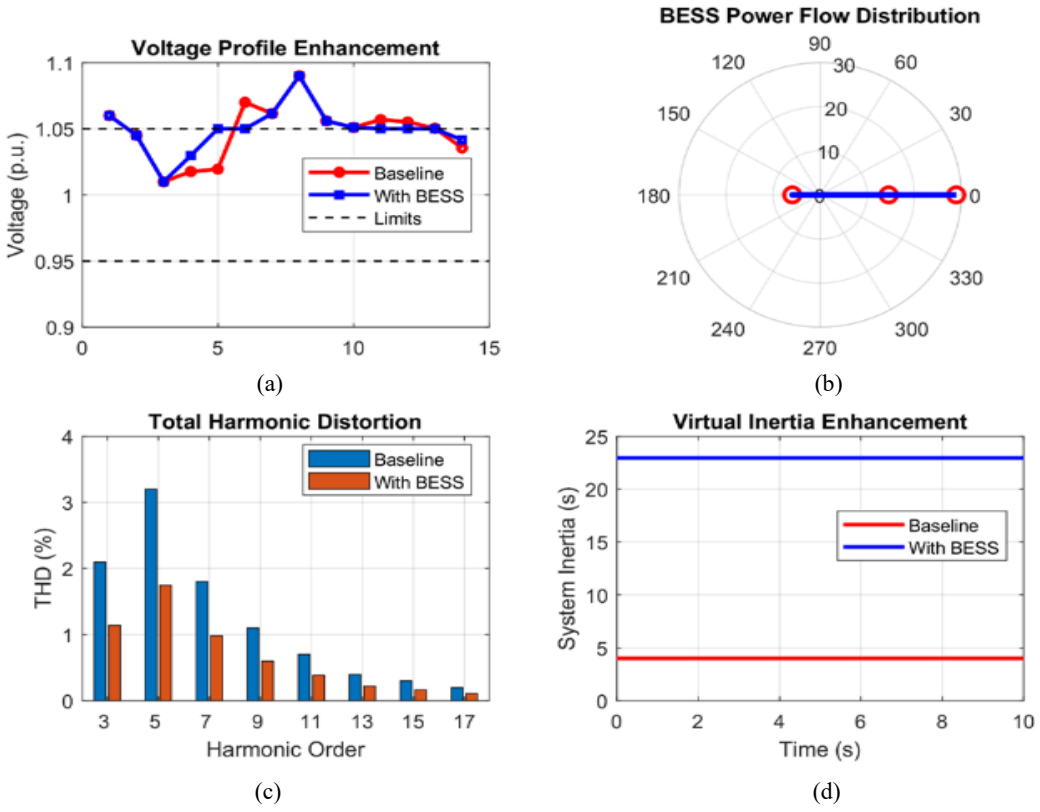

Figure 9 The stability generated from the integration of BESS into the IEEE 14-bus grid with figure (a) showing the voltage enhancement, (b) BESS power flow distribution, (c) Total harmonic distortion in the voltage waveforms, (d) the virtual inertia enhancement.

4.3 IEEE 30-Bus

4.3.1 BESS optimization

In the case of the IEEE 30-bus system, 5 BESS units were optimized, leading to a 40% generation capacity allocation to Bus 18, Bus 9 and Bus 12. In particular, Bus 18 normalized 36.0 MW/92.1 MWh, Bus 9 normalized 26.9 MW/122.4 MWh, and Bus12 normalized 27.6 MW/66.6 MWh in Figures 10(a) and 10(b) respectively, and therefore, they are considered the best places to inject virtual inertia.

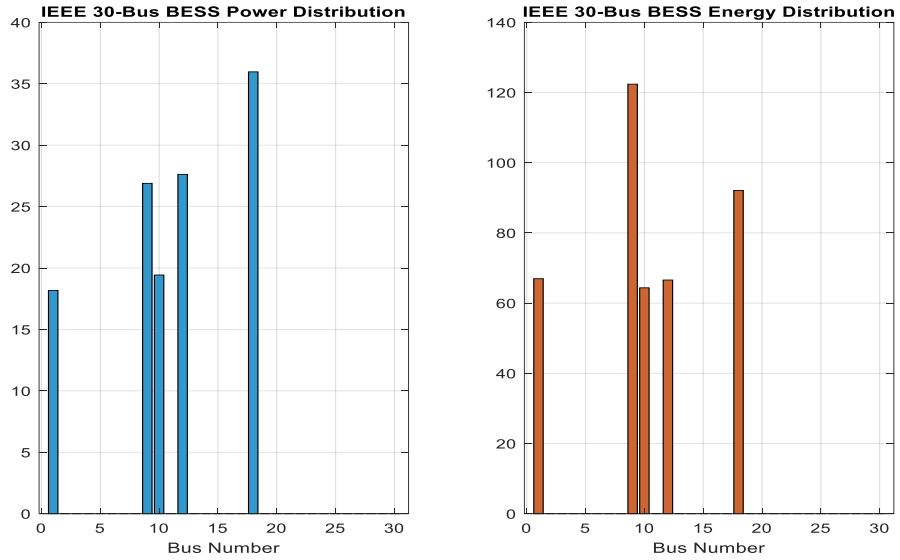

Figure 10 (a) The distribution of BESS power (in MW) and (b) BESS energy distribution (in MWh) across the selected buses in the IEEE 30-bus system

These specific buses were identified as the optimal and effective BESS placement to inject virtual inertia, that stabilized the IEEE 30-bus system transmission network.

4.3.2 TLBO Analysis

The TLBO algorithm reduced the objective function faster compare to the baseline system [12], with an optimization drop from 5.5 to 0.1 on the log scale just after 50 iterations as in Figure 11(a). The resulting decrease in the diversity of the population supported the TLBO's ability to balance search exploration-exploitation. The population diversity evolution in Figure 11(b), highlights the TBLO's characteristic to premature entrapment at local minima, thus allowing for local search optimization at the learning phase. The corresponding convergence rate reduces in a similar trend as in Figure 11(c), thus proving the efficacy of the algorithms. The search exploration to identify the optimal solution increases with the increase in iteration Figure 11(d). Nearly 100% of the parameters were explored, reflecting the robustness of the TBLO algorithm.

4.3.3 Frequency Response

When the optimal BESS solution was placed, the systems showed reduced changes in frequency and RoCoF during disturbances. Without the BESS, the frequency deviation was by a magnitude of 0.4Hz, and beyond the secondary limit as in figure 12(a). However, with the optimal BESS placement, the frequency change occurred within the set limit of $[-1\ 0]Hz$. Thus, ensured faster system stabilization. The RoCOF curve shows slow stabilisation with BESS placement at a constant value of 0.015Hz/s, and a nonlinear curve for the baseline system Figure 12(b). The maximum frequency deviation (Δf) showed significant improvement across contingency scenarios: during a generator outage it reduced from 0.503 Hz to 0.312 Hz; and during a line N-1 loss it reduced from 0.428 Hz to 0.242 Hz. However, during a PV power drop and load increase, the frequency deviation experienced slight increases, indicating varying performance based on the disturbance type. The values represent the change in Nadir frequency for respective baseline cases and that with optimal BESS placement as in Figure 12(c). The optimal location of the BESS thus cleared disturbances after and limited frequency decay. The recovery time was significantly reduced, for instance, case of a generator outage 25s with no BESS, and 8s with BESS as shown in Figure 12(d).

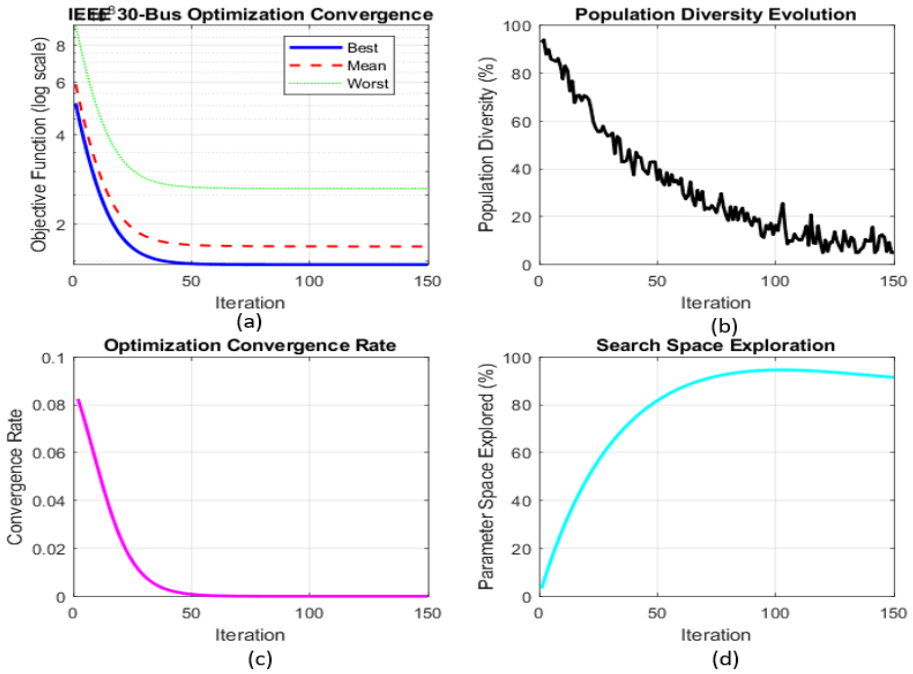

Figure 11 (a)The convergence of the TLBO algorithm, (b) population diversity evolution, (c) convergence rate during optimization and (d) search space exploration

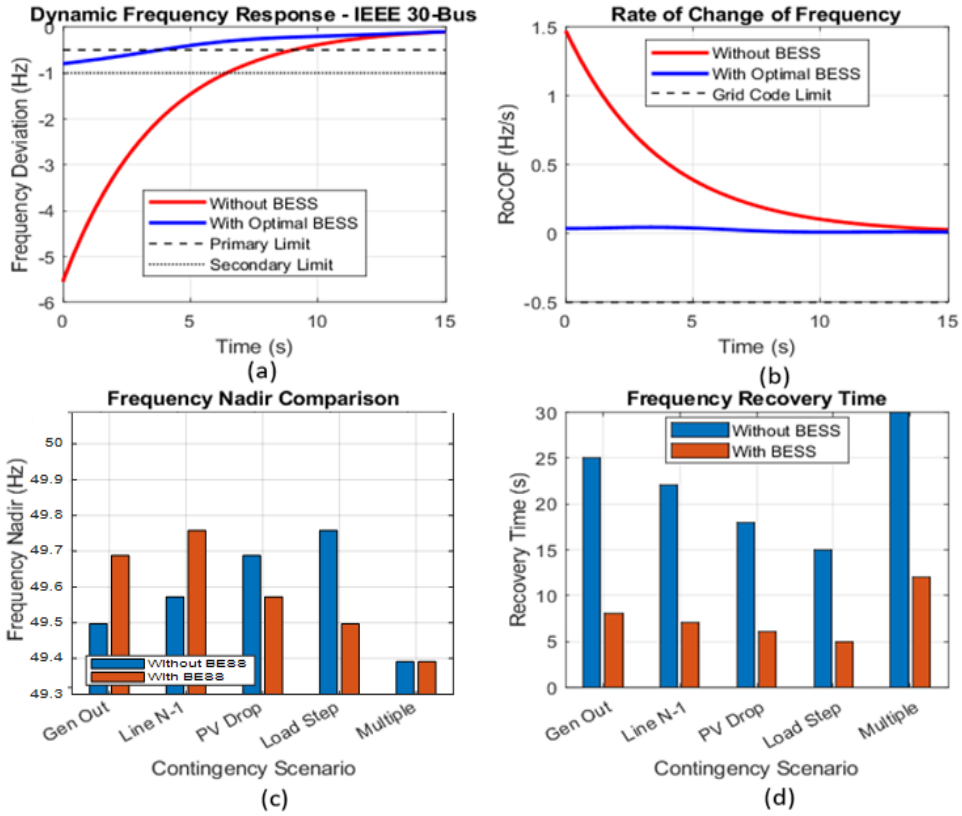

Figure 12 (a) The dynamic frequency response in the IEEE 30-bus system, (b)) the rate of change of frequency, (b) The comparison of Nadir frequency at different contingency scenarios and (d) Frequency recovery at different contingency scenarios.

4.3.4 Reliability and Resilience Metrics

Figure 13(a) contrasts the effect of BESS integration on the essential power system reliability and resilience quality measure and includes SAIDI, SAIFI, CAIDI and ASAI. In the baseline system has a SAIDI of 180 h/yr, SAIFI of 2.5 interruptions/yr, CAIDI of 100 h, and ASAI of 100%. After an optimal BESS placement integration, the following metrics improved: SAIDI decreases to 160 h/yr and SAIFI decreases to 1.1 interruptions/yr. At the same time CAIDI decreases to 98 h and system availability (ASAI) increases to 99 %. Figure 13(b) shows the distributions of outage duration and indicates that the BESS is effective in reducing the number of extended blackout hours. In particular, the number of major outages that take more than 5 hours reduces to 11 per year. The system resilience is also measured by the recovery time curves presented in Figure 13(c). In the baseline system, the performance curve was lower point to insufficient virtual inertia while BESS placement was effective in restoring networks much faster. Figure 13(d) shows that BESS placement is able to deliver specific backup power to vital installations thus withstand loads in hospitals up to 4.3 hours and 3.8 hours in data centers. All in all, these findings suggest that the placement of BESS improves reliability and offers extended backup to priority loads in prolonged grid disturbances.

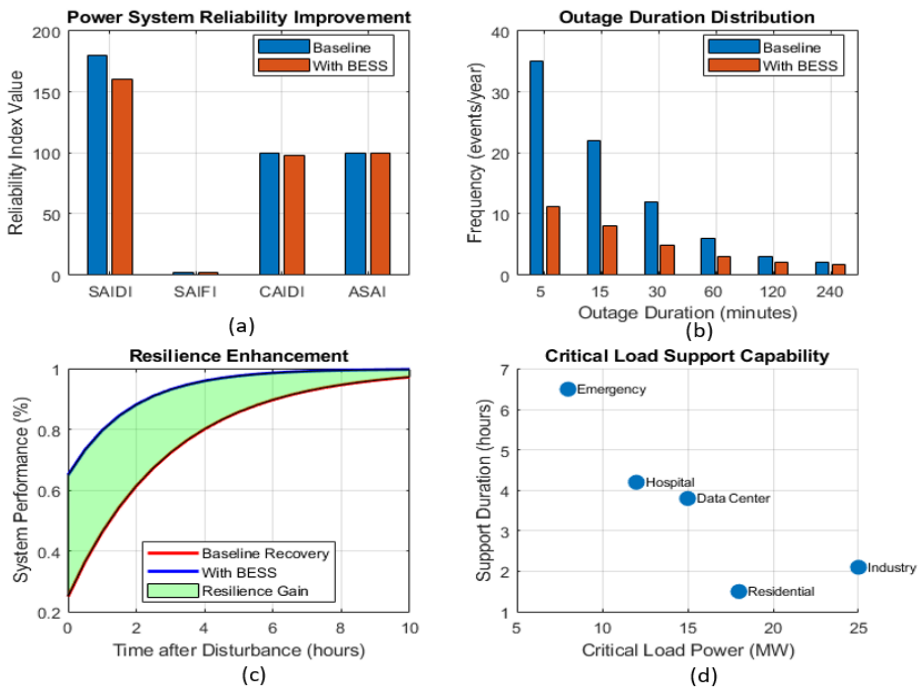

Figure 13 (a)The impact of BESS on system reliability, (b) the outage distribution frequency against the duration of the outage, (c) resilience gain on the IEEE 30-bus system and (d) the critical load support capability.

4.3.5 Stability Metrics

The BESS placement introduced significant improvements in the steady-state and dynamic stability measures of the IEEE 30-bus system with a high PV 40% penetration. As shown in figure 14(a), there is an increase to the local voltage at Bus 18, by 0.128 p.u. to stabilize at 1.04 p.u. This kept the network stability with the typical regulatory limits ranging between o.95-1.05 p.u. Power-flow distribution as is seen in Figure 14(b), depicts a more balanced active power-flow distribution with fewer skewness values observed in the polar plot of the network. The BESS placement thus reduces transmission congestion directly by injecting power at optimized load centers which effectively reduces the maximum branch flow of 130 MW to 110 MW. The total harmonic distortion (THD) represented the power quality introduced by the active-filtering form the BESS inverters. The inverters are shown to respond effectively to voltage harmonics amongst buses with

solar PV interconnection. For example, at Bus 5 the THD of voltage was significantly reduced from 3.2% to 1.8% as seen in Figure 14(c). Virtual Lastly, the virtual inertia emulation showed a positive effect on the system, in terms of resiliency to frequency transients. The effective system inertia was critically undermined before BESS integration with more than 40% of PV penetration. The total system inertia is significantly increased with the BESS placement. For instance, an improvement in the inertia in a baseline of 4.2s to a better 14.5s. This is equivalent to a 33% reduction in the overall system inertia, which effectively counteracted the deficit in mechanical rotating mass.

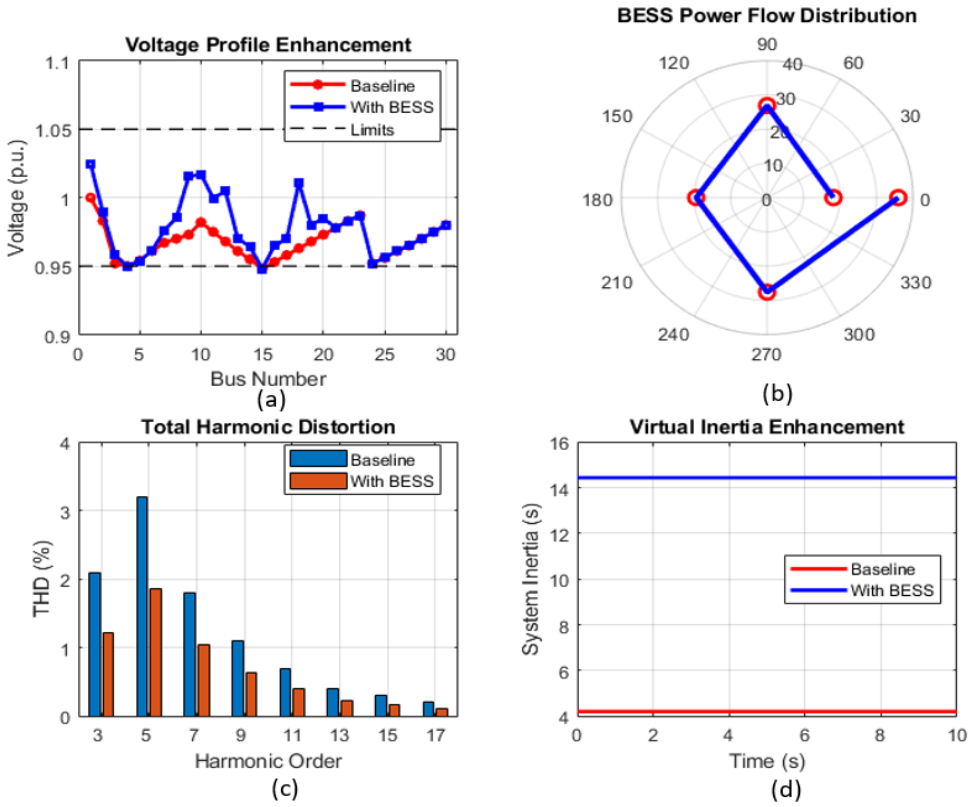

Figure 14 The stability generated from the integration of BESS into the IEEE 30-bus grid with figure (a) showing the voltage enhancement, (b) BESS power flow distribution, (c) Total harmonic distortion in the voltage waveforms and (d) the virtual inertia enhancement.

4.4 Comparison between IEEE 14 and IEEE 30-bus system

A comparative study of the maximum frequency deviation, and the RoCoF, for example, under the condition of a generator outage, has been provided in Table 2. For the IEEE 14-bus, 30-bus systems under five different scenarios, both the baseline and with optimal BESS integration, the maximum frequency deviation under a generator outage, 0.503 Hz and the maximum RoCoF was 0.030 Hz/s. This is an indication that, while the BESS placement provides negligible transient frequency containment for the 14-Bus network under these severe faults, it remains highly valuable for steady-state power quality, localized voltage support, and harmonic filtering. For the IEEE 30-Bus system, during an N-1-line loss the placement reduced the frequency deviation from 0.503 Hz to 0.312 Hz and corresponding RoCoF from 0.030 Hz to 0.019 Hz/s. Similarly, the generator outage reduced the frequency deviation from 0.428 Hz to 0.242 Hz. Nonetheless, in the conditions of the PV power drop and quick increase in the load, the data shows bigger variations in the presence of the BESS placement like the increase in frequency deviation from 0.242 Hz to 0.503 Hz. This indicates that there is possible negative impact due to storage control strategy. Furthermore, during

cascading multiple faults, the metrics remain constant at 0.609 Hz and 0.037 Hz/s, indicating that the BESS inverter capacities become saturated and are unable to arrest the cascading failure.

Table 2 Frequency Stability Performance Comparison for IEEE 14-Bus and 30-Bus test systems

Scenario	14-Bus without BESS Δf (Hz)	14-Bus without BESS RoCoF (Hz/s)	14-Bus with BESS Δf (Hz)	14-Bus with BESS RoCoF (Hz/s)	30-Bus without BESS Δf (Hz)	30-Bus without BESS RoCoF (Hz/s)	30-Bus with BESS Δf (Hz)	30-Bus with BESS RoCoF (Hz/s)
Generator Outage	0.503	0.030	0.503	0.030	0.503	0.030	0.312	0.019
Line N-1 Loss	0.428	0.026	0.428	0.026	0.428	0.026	0.242	0.015
PV Power Drop	0.312	0.019	0.312	0.019	0.312	0.019	0.428	0.026
Load Increase	0.242	0.015	0.242	0.015	0.242	0.015	0.503	0.030
Multiple Faults	0.609	0.037	0.609	0.037	0.609	0.037	0.609	0.037

As observed in Table 2, the integration of BESS into the IEEE 14-bus system yielded negligible transient frequency containment during severe faults, with maximum frequency deviation and RoCoF remaining unchanged at 0.503 Hz and 0.030 Hz/s respectively. This highlights a limitation of the control strategy in smaller, highly stressed grids, where BESS primarily contributes to steady-state power quality rather than transient arresting. Furthermore, in the IEEE 30-bus system during a load increase, the frequency deviation worsened from 0.242 Hz to 0.503 Hz with BESS. This indicates a potential adverse effect due to the BESS inverter control lag or capacity saturation under specific cascading demand bursts, which should be addressed in future real-time control loop designs.

5. Conclusion and Recommendations

This research developed and tested optimization model to size and placement of lithium-ion BESS to improve virtual inertia in grids with large photovoltaic penetration. Using TLBO algorithm, the research addressed limitations inherent with traditional, distinct, sizing and sitting methods. The proposed model trades off Life-Cycle Cost (LCC) and considers the technical requirements, such as frequency deviation and RoCoF limits. Simulated results on modified IEEE 14-bus and IEEE 30-bus test systems illustrate enhanced stability. In the case of the IEEE 14-bus test system, TLBO algorithm optimally placed three BESS units, with highest capacity on Bus 8. Nevertheless, the system successfully increased voltage profiles at weak nodes, minimizing the voltage Total Harmonic Distortion (THD) by an estimated 16 percent. With the IEEE 30-bus case, the optimal BESS placement reduced the maximum frequency deviation from 0.503 Hz to 0.312 Hz, while maintaining the RoCoF within the typical grid limit of ± 1Hz/s when the generator outage disturbance was introduced. The BESS placement also introduced virtual inertia, increasing the effective system inertia constant by 33%, besides reducing the recovery time of the frequency from 25 seconds to 8 seconds. Furthermore, the grid reliability indicators showed significant improvement, with the SAIDI index decreasing by 65%. This shows an increase in resiliency of the proposed algorithm. TLBO algorithm was also found to depend on limited parameter and converged after 50 iterations.

It is recommended that the grid systems with over 40% renewable integration should use simultaneous size

and BESS placement optimization models, to minimize Life-Cycle Costs. Even though lithium-ion BESS has been shown effective in rapid frequency response, further research needs to extend the study to Hybrid Energy Storage Architectures (HESS) systems. This combination of lithium-ion batteries with Supercapacitors or flywheels, to optimize the compromise between the inertial response power density and the long outage energy density. Lastly, future research needs to incorporate real-time control loop simulations to test the sub-second Virtual Inertia Emulation response of the optimal configurations.

For grid operators and policymakers, this study provides a practical, scalable framework for transitioning toward high-renewable grids. By utilizing the simultaneous TLBO sizing and placement strategy, operators can avoid over-capitalizing on oversized BESS infrastructure, while strategically targeting weak grid nodes. This ensures regulatory compliance for frequency stability without requiring massive physical transmission upgrades.

Declaration of Ethical Standards

As the authors of this study, we declare that he complies with all ethical standards.

Credit Authorship Contribution Statement

Eng. Kaveke Kiima: Conceptualization, Methodology, Software, Validation, Formal analysis, Investigation, Writing original Draft, Visualization

Dr. Irene Muisyo: Conceptualization, Methodology, Validation, Writing-Review and Editing, Supervision

Dr. Linus Aloo; Methodology, Validation, Writing-Review and Editing, Supervision

Declaration of Competing Interest

The authors declared that they have no conflict of interest.

Funding / Acknowledgements

This research received no specific grant from any funding agency in the public, commercial, or non- profit organizations

Data Availability

The data that support the findings of this study are available from the corresponding author upon reasonable request

References

Abbawi, A., Ismael, I., & Alyozbaky, O. S. (2020). Comparison between two methods to analyze multiple faults in IEEE 14-bus. In 2020 7th International Conference on Electrical and Electronics Engineering (ICEEE) (pp. 188–193). https://doi.org/10.1109/ICEEE49618.2020.9102491.

Abdel-Basset, M., Abdel-Fatah, L., & Sangaiah, A. K. (2018). Metaheuristic algorithms: A comprehensive review. In Computational intelligence for multimedia big data on the cloud with engineering applications (pp. 185–231). Elsevier. https://doi.org/10.1016/B978-0-12-813314-9.00010-4.

Adetokun, B. B., Oghorada, O., & Abubakar, S. J. (2022). Superconducting magnetic energy storage systems: Prospects and challenges for renewable energy applications. Journal of Energy Storage, 55, 105663. https://doi.org/10.1016/j.est.2022.105663.

Alam, M., et al. (2022). Frequency stabilization of AC microgrid clusters: An efficient fractional order supercapacitor controller approach. Energies, 15(14), 5179. https://doi.org/10.3390/en15145179

Ayamolowo, O. J., Manditereza, P. T., & Kusakana, K. (2022). Optimal planning of renewable energy generators in modern power grid for enhanced system inertia. Technology and Economics of Smart Grids and Sustainable Energy, 7(1), 33. https://doi.org/10.1007/s40866-022-00157-8.

Cai, Z., et al. (2022). Multistage bilevel planning model of energy storage system in urban power grid considering network reconfiguration. Frontiers in Energy Research, 10, 952684. https://doi.org/10.3389/fenrg.2022.952684.

Carpinelli, G., Noce, C., Russo, A., Varilone, P., & Verde, P. (2024). Optimal siting and sizing of battery energy storage systems in unbalanced distribution systems: A multi objective problem under uncertainty. International Journal of Electrical Power & Energy Systems, 162, 110316. https://doi.org/10.1016/j.ijepes.2024.110316.

Cole, W., & Karmakar, A. (2023). Cost projections for utility-scale battery storage: 2023 update. National Renewable Energy Laboratory. https://docs.nrel.gov/docs/fy23osti/85332.pdf.

Deng, X., et al. (2023). Review of RoCoF estimation techniques for low-inertia power systems. Energies, 16(9), 3708. https://doi.org/10.3390/en16093708.

Fernandez, L. M., Garcia, C. A., Saenz, J. R., & Jurado, F. (2006). Reduced model of DFIGs wind farms using aggregation of wind turbines and equivalent wind. In 2006 IEEE Mediterranean Electrotechnical Conference (MELECON) (pp. 881–884). https://doi.org/10.1109/MELCON.2006.1653239.

Golpîra, H., et al. (2020). Optimal energy storage system-based virtual inertia placement: A frequency stability point of view. IEEE Transactions on Power Systems, 35(6), 4824–4835. https://doi.org/10.1109/TPWRS.2020.3000324.

IEEE. (2020). IEEE recommended practice for improving the reliability of emergency and standby power systems. https://doi.org/10.1109/IEEESTD.2020.9205732.

International Energy Agency. (2023). Renewables 2023: Analysis and forecast to 2028. https://iea.blob.core.windows.net/assets/96d66a8b-d502-476b-ba94-54ffda84cf72/Renewables_2023.pdf.

International Renewable Energy Agency. (2025). Renewable capacity statistics 2025. https://www.irena.org/-/media/Files/IRENA/Agency/Publication/2025/Mar/IRENA_DAT_RE_Capacity_Statistics_2025.pdf.

Islam, B. U., Baharudin, Z., & Kattel, P. (2021). Inertia theory frequency dynamic analysis and control of power system with high proportion of renewable source. Mathematical Problems in Engineering, 2021, 1–16. https://doi.org/10.1155/2021/9472957.

Jaradat, T., & Khatib, T. (2025). Optimal sizing of battery energy storage system in electrical power distribution network. Energy Exploration & Exploitation, 43(3), 909–931. https://doi.org/10.1177/01445987241300183.

Julius, N., Nderu, J. N., & Irungu, G. K. (2019). Frequency control and virtual inertia emulation techniques for grid connected wind energy conversion systems: A review. In 2019 IEEE AFRICON (pp. 1–6). https://doi.org/10.1109/AFRICON46755.2019.9133975.

Lybbert, M., Ghaemi, Z., Balaji, A. K., & Warren, R. (2021). Integrating life cycle assessment and electrochemical modeling to study the effects of cell design and operating conditions on lithium-ion batteries. Renewable and Sustainable Energy Reviews, 144, 111004. https://doi.org/10.1016/j.rser.2021.111004.

Neto, P. J. D. S., et al. (2020). Power management strategy based on virtual inertia for DC microgrids. IEEE Transactions on Power Electronics, 35(11), 12472–12485. https://doi.org/10.1109/TPEL.2020.2986283.

Piccoli, D. C., Trentini, R., & Saldanha, J. J. A. (2021). Synchronous inertia deficit: A study on electric power systems with high penetration of renewable energy sources. In 2021 9th International Conference on Systems and Control (ICSC) (pp. 56–61). https://doi.org/10.1109/ICSC50472.2021.9666536.

Rao, R. V., & Patel, V. (2013). Comparative performance of an elitist teaching-learning-based optimization algorithm for solving unconstrained optimization problems. International Journal of Industrial Engineering Computations, 4(1), 29–50. https://doi.org/10.5267/j.ijiec.2012.09.001.

Shahjalal, M., et al. (2022). A review on second-life of Li-ion batteries: Prospects, challenges, and issues. Energy, 241, 122881. https://doi.org/10.1016/j.energy.2021.122881.

Subasinghage, K., et al. (2022). Modern supercapacitors technologies and their applicability in electrical engineering applications. Energies, 15(20), 7752. https://doi.org/10.3390/en15207752.

Swetala, E. G., Kaberere, K. K., & Munda, J. L. (2025). Offline estimation of power system inertia distribution. e-Prime – Advances in Electrical Engineering, Electronics and Energy, 11, 100923. https://doi.org/10.1016/j.prime.2025.100923.

Tamrakar, U., et al. (2017). Virtual inertia: Current trends and future directions. Applied Sciences, 7(7), 654. https://doi.org/10.3390/app7070654.

Tercan, S. M., et al. (2021). An expansion planning method for extending distributed energy system lifespan with ESS. https://doi.org/10.20944/preprints202101.0020.v1.

Xie, C., et al. (2021). Optimal sizing of battery energy storage system in smart microgrid considering virtual energy storage system and high photovoltaic penetration. Journal of Cleaner Production, 281, 125308. https://doi.org/10.1016/j.jclepro.2020.125308.

Zakeri, A., & Askarian Abyaneh, H. (2017). Transmission expansion planning using TLBO algorithm in the presence of demand response resources. Energies, 10(9), 1376. https://doi.org/10.3390/en10091376.